Chemistry–A European Journal

Research Article
doi.org/10.1002/chem.202501897

Chemistry Europe
European Chemical Societies Publishing

www.chemeurj.org

High Dispersion of Copper Nanoparticles on Carbon Black in Minimal Loadings Enhances the Electroreduction of CO_2 to CO

Eduardo Henrique Dias,[a, b, c] Gelson Tiago dos Santos Tavares da Silva,[c, d] Cao-Thang Dinh,[c] Khac Huy Dinh,[c] Lucia Helena Mascaro,[d] and Caue Ribeiro*[b]

Electrochemical CO_2 reduction (ECR) offers a promising route for converting CO_2 emissions into valuable chemicals. To enhance economic viability, the development of efficient and low-cost catalysts based on nonnoble metals is crucial. This study focuses on copper (Cu) nanoparticles highly dispersed on a carbon black (CB) support, synthesized via a solvothermal method that allows for precise control over particle size and loading. We demonstrate that tuning these properties is essential to steer the selectivity of CO_2 reduction toward carbon monoxide (CO). Notably, a low catalyst loading of only 0.159 mg/cm^2 was sufficient to achieve high performance. The optimized catalyst delivered a CO partial current density of 66 mA/cm^2 (total current density of 100 mA/cm^2 with 66% Faradaic efficiency (FE) for CO) at a cell voltage of 3.2 V. Furthermore, our results highlight the critical role of the gas diffusion layer (GDL), showing that its composition significantly impacts catalyst activity. This underscores the necessity of engineering advanced GDLs with tailored conductivity, stability, and hydrophobicity to further boost the performance of Cu-based catalysts in CO_2 electrolysis.

1. Introduction

The conversion of carbon dioxide (CO_2) into valuable products has become an increasingly important field of research due to the need to reduce carbon emissions and address climate change.[1–3] Electrochemical CO_2 reduction (ECR) is considered a sustainable and promising approach to mitigating the carbon footprint. By utilizing renewable electricity to efficiently convert CO_2 into valuable platform molecules for fuels and chemicals, it has the potential to achieve net-zero or even negative carbon emissions.[4] Despite significant advances, scaling laboratory results to practical applications remains a chronic difficulty since both the design and scalability of the catalyst must be adjusted to maintain high performance while reducing the cost for catalyst fabrication.[5]

Cu-based catalysts have attracted considerable attention in ECR due to their unique ability to promote the effective conversion of CO_2.[6] However, the moderate attraction of the reaction intermediates (i.e., *CO, *CHO, *CH_2O, etc.) to the Cu surface leads to poor product selectivity.[7] Iyengar et al. showed that to better control Cu selectivity in conventional systems, it requires fine-tuning of the structure, shape, and size of the catalyst particles.[8] The trends and mechanisms observed at low currents ($<$ 10 mA/cm^2) may not hold at higher current densities ($\geq$ 100 mA/cm^2) due to factors like mass transport and local pH variations.[9]

The selectivity of a material strongly depends on its active sites, which correlate with its preferred crystal orientation and particle size.[10] Studies have shown that oxide-derived Cu contains at least three types of active sites,[11] each specializing in the selective production of ethylene, ethanol/acetate, or 1-propanol. In our study, different Cu nanoparticles with different ratios were prepared, indicating a preference for planes (111) and (100). Based on the literature, the cubic sample predominantly exposed the (100) plane, while the octahedral sample exposed the (111) plane, and the spherical sample showed a mixture of both planes. This greater exposure directly affected the reaction selectivity: the (100) and (111) surfaces promoted the formation of ethylene and methane, respectively, whereas the spherical sample did not exhibit notable selectivity. The selectivity of Cu-based catalysts can also be manipulated to obtain CO as the main product by reducing particle sizes and increasing the catalyst dispersion on the support electrode.[12] This increases the transportation of CO_2 and CO* intermediates. When combined with a highly dispersed, low-content nanometric catalyst in the

[a] E. H. Dias
Institute of Chemistry of São Carlos - IQSC, University of São Paulo, Av. Trab. São Carlense, 400 – Parque Arnold Schimidt, São Carlos, São Paulo 13566-590, Brazil

[b] E. H. Dias, C. Ribeiro
National Nanotechnology Laboratory for Agrobusiness – LNNA, Embrapa Instrumentation, Rua XV de Novembro, 1452–Centro, São Carlos, São Paulo 13561-206, Brazil
E-mail: caue.ribeiro@embrapa.br

[c] E. H. Dias, G. T. dos S. T. da Silva, C.-T. Dinh, K. H. Dinh
Department of Chemical Engineering, Queen's University, 19 Division Street, Kingston, Ontario K7L 3N6, Canada

[d] G. T. dos S. T. da Silva, L. H. Mascaro
Department of Chemistry, Federal University of São Carlos, Rod. Washington Luiz, Km 205, São Carlos–SP, Brazil

Supporting information for this article is available on the WWW under https://doi.org/10.1002/chem.202501897

system, the distance between catalytic sites increases, reducing the probability of C—C coupling and improving the CO release.[13]

The performance of ECR is also highly influenced by the interaction between Cu and the conductive support. For instance, carbon-supported Cu nanocatalysts have demonstrated better selectivity for C_2H_4 compared to electrodeposited Cu.[14–16] In this aspect, carbon is a promising material as a support for Cu catalysts because it can help stabilize the nanoparticles and prevent agglomeration during the reaction.[17] However, the size and distribution of synthesized nanoparticles directly on carbon supports, as well as their performance for CO_2 conversion, still require investigation to define the optimal conditions for catalyst preparation.

To establish optimal conditions for maximizing performance, stability, sustainability, and scalability, the careful selection of catalyst loading and deposition method is essential and has a significant impact on overall efficiency.[18–20] Catalyst loading can be optimized to reach an ideal balance, ensuring minimal use of metal resources, which contributes to sustainability and reduces the final system cost for scaled-up systems. Additionally, catalyst loading plays a significant role in determining ECR performance.[21,22] For example, Cu selectivity can be modulated by controlling particle size and distribution.[23] It is even more critical to achieve high dispersion without agglomeration for nanoparticles, as agglomeration can occur following current application. Maintaining nanoparticles separated from each other favors CO formation, as it reduces the probability of C—C bond formation.[24] However, if catalyst loading is excessively minimized, issues such as increased resistivity, shifts in reaction preference, and insufficient availability of catalytic sites can arise, potentially rendering the catalyst inefficient. Although silver-based materials are widely used due to their selectivity for CO production, silver is significantly more expensive compared to Cu and has a higher overpotential than Cu. Therefore, if Cu-based catalysts can be developed with high selectivity specifically for CO production, they would represent a much more viable alternative due to their lower cost and abundance.

In this work, we investigated the role of Cu dispersion on carbon black (CB) supports, focusing on low Cu contents for CO production. CB, widely used as support for hydrogen evolution catalysts, provides a high surface area, stability, and excellent conductivity. It is an ideal candidate for use as a substrate to improve the homogeneity of catalyst distribution and to stabilize catalyst particles.[25,26] Furthermore, the use of solvothermal treatment enables the synthesis of a highly distributed material with more homogeneous particle sizes. Our results show that high catalyst dispersion is critical to achieving high efficiency in membrane electrode assembly (MEA) cells using low catalyst amounts (0.159 mg/cm^2). The high dispersion led to high currents (> 100 mA/cm^2) at acceptable cell potentials (below -3.2 V) and FE values (>60% for CO) despite the significantly lower Cu content compared to the literature that normally presents electrodes with 1–5 mg/cm^2 of catalyst loading to achieve current densities of 50–150 mA/cm^2.[27,28]

2. Results and Discussion

Copper oxide (CuO) was used as the starting material because it has been widely used for CO_2 reduction.[29] CuO supported on carbon (C.CuO) was prepared by the solvothermal method by mixing appropriate amounts of CB and Cu acetate into an ethanol solution. This technique enables precise control over particle morphology, size, and distribution by adjusting parameters such as temperature, reaction time, solvent selection, and other factors.[30] The mixture was thermally treated at 110 °C for 12 hours. The crystal nucleation and particle size are affected by the concentration of metal salt in the solution[30] Thus, catalyst loading and particle size were adjusted by varying the percentage of Cu acetate added to the solution, while maintaining a constant CB weight across all samples.

The crystalline phases of both catalyst and support were characterized using X-ray diffraction (XRD). As seen in Figure 1, all prepared samples showed the same main diffraction peaks at 2θ values of 36°, 38°, and 48°, which correspond to the reflections of the (-111), (111), and (-222). These peaks are indexed to the tenorite phase of CuO (COD ID: 9 015 924). It is worth mentioning that no other Cu species (Cu_2O and Cu^0) were identified. The broadband at $2\theta = 25°$ found in all the diffractograms analyzed (Figure 1) can be associated with the hexagonal structure of the CB.[31] In addition, peak intensities of the CuO phase in the XRD patterns increase as the CuO loading increases. The expected mass of CuO in the catalyst powder was calculated prior to the synthesis. To achieve the desired percentage of CuO (m_{CuO}/m_{total}), we fixed 1 g of CB and used the following equation to determine the mass of CuO:

$$\frac{m_{CuO}}{m_{Carbon} + m_{CuO}}.100 = CuO\ \% \quad (1)$$

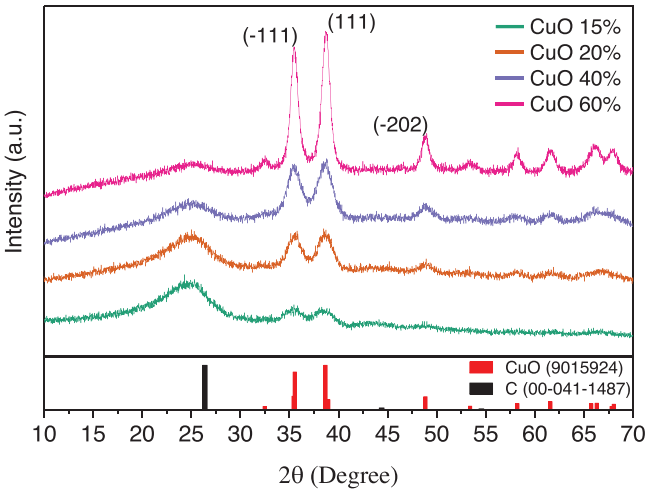

Figure 1. XRD analysis for all CuO percentages onto carbon. The diffraction patterns of the tenorite phase of copper oxide (red) and carbon (black) were also included as a reference.

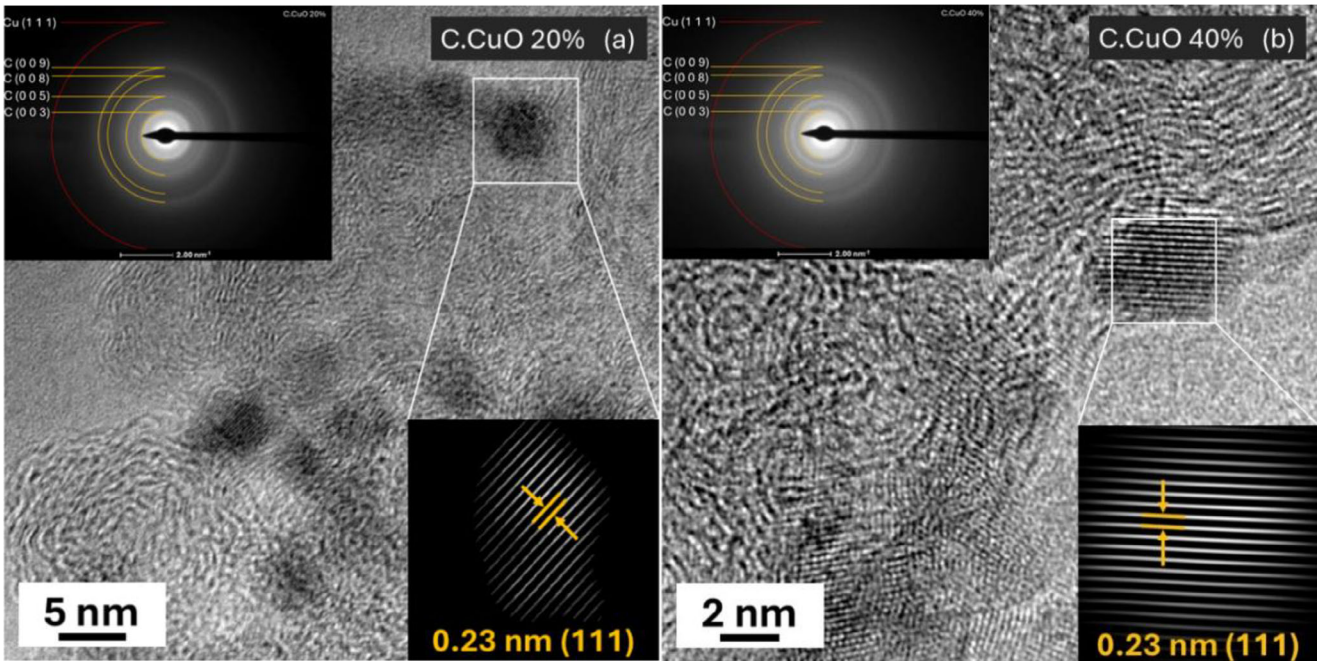

Figure 2. High-Resolution Transmission Electron Microscopy (HRTEM) images of the prepared Cu-based catalysts. a) HRTEM micrograph of the C.CuO 20% catalyst and b) HRTEM micrograph of the C.CuO 40% catalyst. For each image, the top-left insets correspond to Selected Area Electron Diffraction (SAED) patterns, which confirm the crystalline nature of the nanoparticles with characteristic diffraction rings indexed to the (111), (009), (005), and (003) planes. The bottom-right insets are magnified views of the lattice fringes, demonstrating an interplanar spacing of approximately 0.23 nm, which is consistent with the (111) planes of CuO and highlights the high crystallinity of the nanoparticles.

Considering that all the Cu acetate used for synthesis would be converted to CuO, we calculated the necessary mass of Cu acetate to obtain the correct percentage of CuO.

Thermogravimetric Analysis (TGA) and Differential Scanning Calorimetry (DSC) results (Figure S1) show that the variation between the calculated and obtained Cu load can be neglected, confirming that the expected catalyst percentages were successfully obtained. Additionally, the samples with lower Cu loadings exhibit broader diffraction peaks compared to those with higher Cu contents. Beyond reducing the Cu loading, the employed method may also influence other sample characteristics, such as crystallinity and particle size.[32] The broadening effects observed in the XRD peaks with decreasing CuO percentages are not due to a loss of crystallinity but rather result from the presence of fewer nanoscale particles, which cause this broadening in the material's signal.[33]

To further characterize the crystalline structures and morphologies of CuO particles, high-resolution transmission electron microscopy (HRTEM) and scanning electron microscopy (SEM) were employed. Both methods show that the particles have a quasi-spherical shape (Figure 2, S2), characteristic of particles synthesized by a high-pressure solvothermal method.[34–36] Particle sizes were measured using images obtained from the dark field technique, which provides a clear measurement of the synthesized particles (Figure 3). The results in Figure 3b show that samples with 20% Cu have particle sizes ranging from 2 to 5 nm. While in Figure 3d, samples with 40% Cu exhibit larger nanoparticles ranging from 3 to 7 nm. The diffraction patterns obtained from the Selected Area Electron Diffraction (SEAD) technique in Figure 2, Table S1, 2, show the preferential crystal orientation (111) obtained for both samples. HRTEM analysis also revealed particles with a lattice spacing of 0.23 nm, which corresponds to the (111) plane of the tenorite lattice obtained from SAED, confirming that the particles measured are CuO.[37]

The presence of CuO was further confirmed by the line scan technique (Figure S4), which revealed simultaneous detection of both Cu and oxygen as the beam intersected the nanoparticles. These observations further reveal the well-defined crystalline planes of prepared particles, confirming that the broadening of the Cu diffraction peaks (Figure 1) can be associated with the small particle size.[32]

The representative SEM images illustrate the tendency of CuO nanoparticles to agglomerate with high Cu content (Figure S1). On the other hand, samples prepared with lower Cu content and greater dispersion exhibit smaller particle sizes. At low concentrations of Cu ions, before the particles fully crystallize, the ions are more evenly distributed and farther apart on the carbon surface. This homogeneous distribution and spacing lead to the creation of more nucleation sites and prevent accumulation that could otherwise result in particle growth or agglomeration. Additionally, the higher number of small nanoparticles, resulting from the low Cu concentration, promotes the formation of more particles on the carbon surface. This leads to the direct crystallization of these particles and increases physical interaction between the materials, enhancing the electronic transfer between the catalytic site and carbon. This improvement could boost the performance of the catalyst's active sites and promote more effective electrochemical reactions.

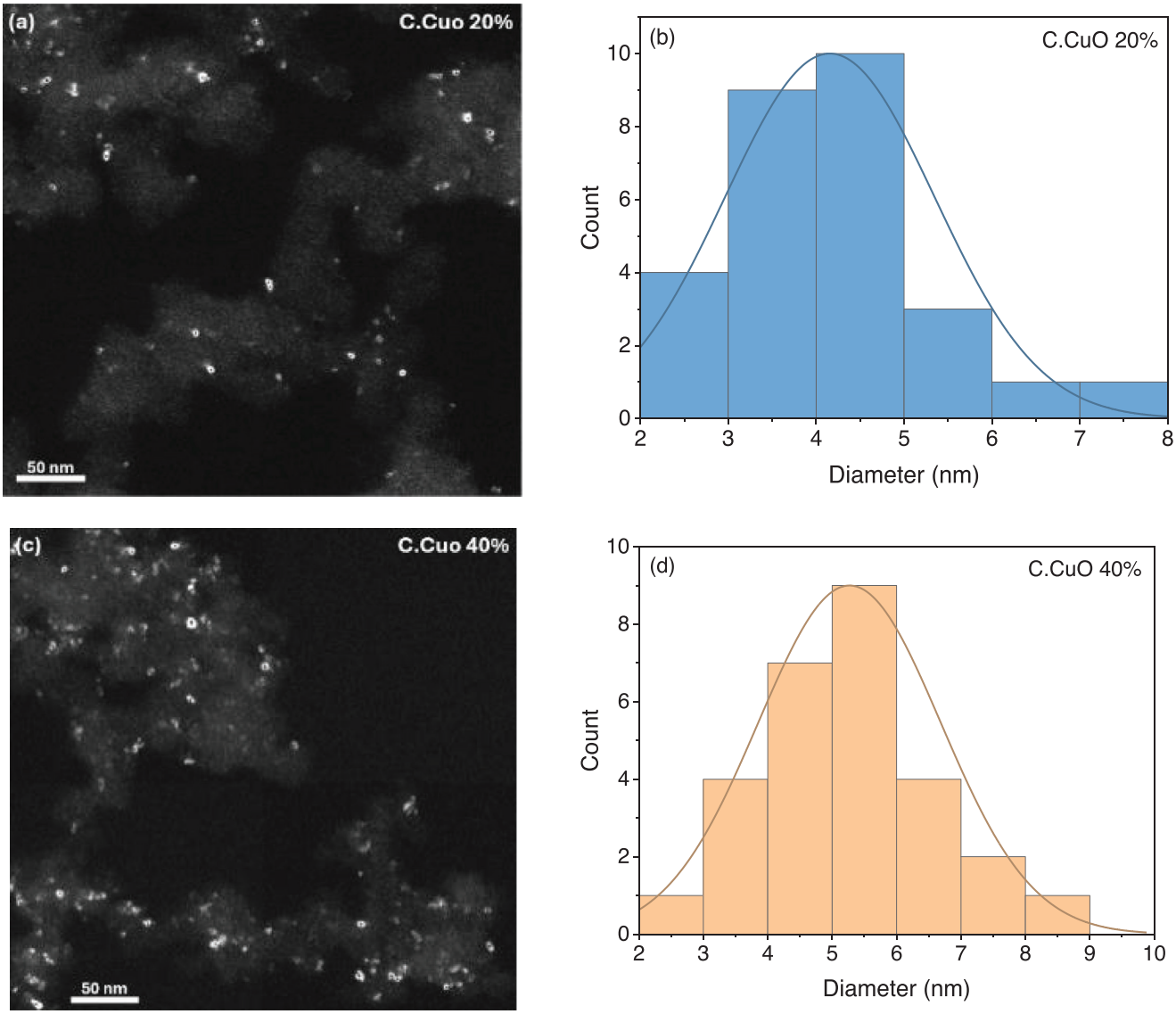

Figure 3. Dark-field microscopy images and corresponding particle size distributions for Cu-based catalysts. a) and c) are dark-field images illustrating the dispersion of nanoparticles on the CB support for C.CuO 20% and C.CuO 40%, respectively. b) and d) are the corresponding particle size distribution histograms for C.CuO 20% and C.CuO 40%, respectively, derived from image analysis.%.

2.1. Electrochemical CO2RR

The ECR performance of the synthesized samples was evaluated using a MEA setup. The prepared C.CuO supported on carbon GDLs (Gas Diffusion Layers) were directly assembled with an Anion Exchange Membrane (AEM) and a Ti/IrO_2 anode (Figure S9). Figure 4a shows the Faradaic efficiency (FE) of reference CB (C) compared to samples prepared with different C.CuO load in the applied current range of 10 to 100 mA/cm^2. The hydrogen is the dominant product on bare CB sample, confirming that Cu is the main active phase in C.CuO catalysts.

Due to the uniform distribution of nanoparticles, when the Cu content in the material falls below 10%, the system starts to favor hydrogen formation (Figure S5). At low Cu concentrations, the carbon surface exposed is significantly higher. This explains the preference for hydrogen production, as carbon promotes this pathway. On the other hand, Cu loadings starting at 15% and higher show a clear shift in selectivity toward CO, diverging from the hydrogen evolution pathway observed at lower concentrations, with a maximum FE for CO (FE_{CO}) of 60% at 50 mA/cm^2 for C.CuO 20%. CO emerges as the primary product in these electrochemical processes. However, a decrease in FE_{CO} is observed as the current density increases. It might be due to the number of active sites on the catalyst capable of converting CO_2 (Cu sites) into products is not enough to utilize the applied current in the system fully. Consequently, when the current exceeds the capacity of the catalytic sites, the system has no alternative but to produce hydrogen over the carbon sites. Moreover, when the Cu percentage is increased to 20% or more, the FE_{CO} does not decrease as significantly with increasing current density compared to the 15% Cu sample, which supports the previous hypothesis.

Increasing the Cu concentration in the catalyst caused particle aggregation during material synthesis, which increased

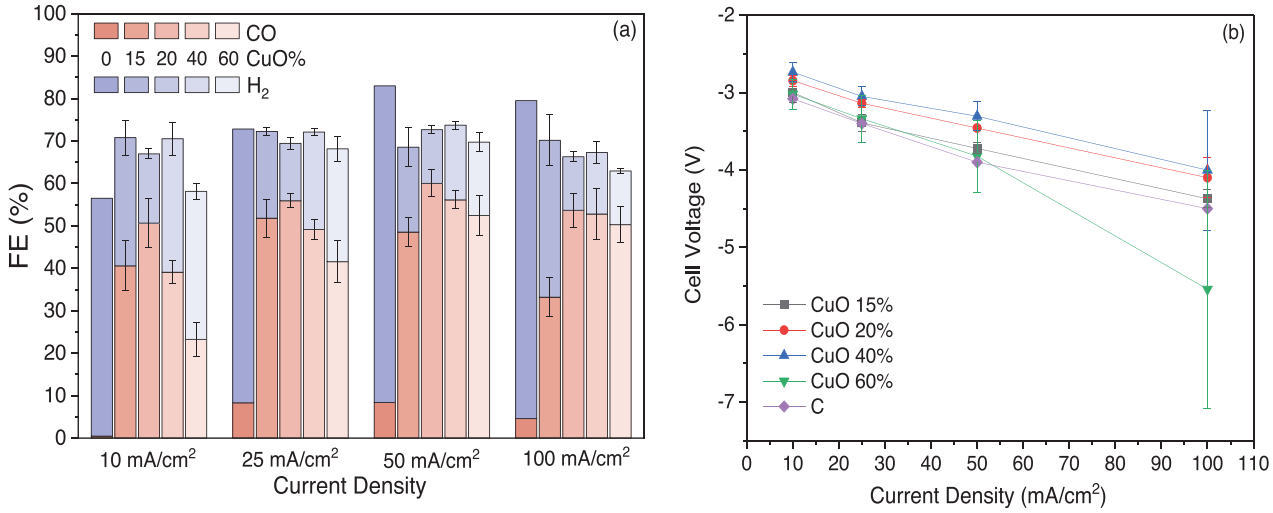

Figure 4. Electrochemical CO_2RR in the AEM – MEA cell using 0.1 M $KHCO_3$ as anolyte and IrOx/Ti-felt as anode. a) Faradaic efficiencies obtained using different Cu loadings onto carbon and b) the respective cell voltages. The error bars represent SD (n = 3 independent replicates). The experiment using bare carbon was performed once only for comparative effect.

particle sizes and reduced the catalyst surface area, ultimately diminishing catalyst activity. The optimum Cu loading is 20%, where the highest selectivity was observed at a current density of 50 mA/cm^2, yielding FE_{CO} = 60% (j_{CO} = 30 mA/cm^2). The calculated amount of metallic Cu in 1 mg of catalyst is 2.51 mmols, corresponding to 0.159 mg, while the C amount is 0.841 mg. Thus, the catalyst activity is determined to be 314 A/gcat. Moreover, in terms of current conversion to products, the most favorable outcome occurred at a current density of 100 mA/cm^2, resulting in FE_{CO} = 53.7% and j_{CO} = 53.7 mA/cm^2, as shown in Figure 4a. This is because even when the current was doubled (from 50 to 100 mA/cm^2), the FE was only slightly reduced. Notably, at this current density, we also observed ethylene (C_2H_4) formation, with 10% of FE.

At a higher current density of 250 mA/cm^2, the catalyst selectivity was changed to ethylene production (Figure S6). The catalysts with 20, 40, and 60% showed FE_{C2H4} around 25, 23, and 21% and FE_{CO} around 25, 22, and 27%, respectively.

As shown in Figure 4b, the cell voltage increases as the current density increase. The cell voltage is not significantly affected by the Cu content in the C.CuO electrodes, showing lower values for C.CuO 20% and 40%. At 100 mA/cm^2 the voltage cell variation is very high and the reason is due to high oxygen formation on the anode electrode, causing the stacked gas in the flow channel and titanium felt, increasing the resistivity and consequently the potential. The catalyst with the best performance, GDL@C.CuO 20% was used for a stability test at 100 mA/cm^2 for 24 hours, Figure 5.

The stability test shows that during the initial phase (first 6 hours), the FE_{H2} was kept close to 15%, while the CO_2 reduction products changed from FE_{CO} = 66% to 45% and FE_{C2H4} = 9% to 19%. From this point, the H_2 production starts to increase while the C_{1+} products decrease. After 14 hours, the FE_{H2} achieved 53.9%, while the FE_{C1+} was lower than 35% (FE_{CO} = 13.6% and FE_{C2H4} = 19.8%). Even with high hydrogen production, the experiment was kept running to evaluate when the system would achieve equilibrium and if the H_2 production would keep increasing. After 24 hours, the H_2 production was extremely low, around 7%, while the FE_{CO} = 37%, and no ethylene was detected. The total gas FE decreased from around 89% to 44%, which means that liquid products could have been formed. This hypothesis was confirmed by washing the electrode with 10 mL of highly pure water to leach the liquid products from the GDL electrode pores, cleaning the flow channel, and solubilizing the possible formed salts. After 1 hour, the results for gaseous products were similar to those obtained before the electrode washing, FE_{H2} = 7% and FE_{CO} = 31%. To collect the liquid products formed during the last hour, the electrode was washed again, passing 10 mL of Milli-Q water through the flow channel to clean the products that might have accumulated in the line and on the electrode. The liquid products carried by the gas stream in vapor form were collected by bubbling the gas outlet into a flask with water and combined with the collected solution. Figure S7 shows the Nuclear Magnetic Resonance (NMR) spectrum for collected liquid products. Formate, ethanol, acetate, and propanol were detected. However, as inserted in Supporting Information, part of the liquid products formed were kept in the flow channel and the carbon GDL, making the FE evaluation difficult. Based on the stability results obtained using carbon GDL, the reason for the substantial change in the total gas FE is not due to some loss in catalyst activity but to the hydrophilicity increase of the carbon GDL over time. This change causes more water to enter the GDL, favoring H_2 production due to electrode flooding. It also decreased the CO_2 availability and favored liquid products. Another noteworthy observation is the decrease in H_2 after 24 hours, which may be related to changes in the microenvironment caused by the increase in local pH due to the formation of ^-OH and the accumulation of carbonates, shifting the selectivity toward liquid products.

To address the hydrophilicity issue, the catalyst was sprayed onto a PTFE substrate, which is hydrophobic, to prevent water flooding.[38] To maintain similar conductivity, a higher amount

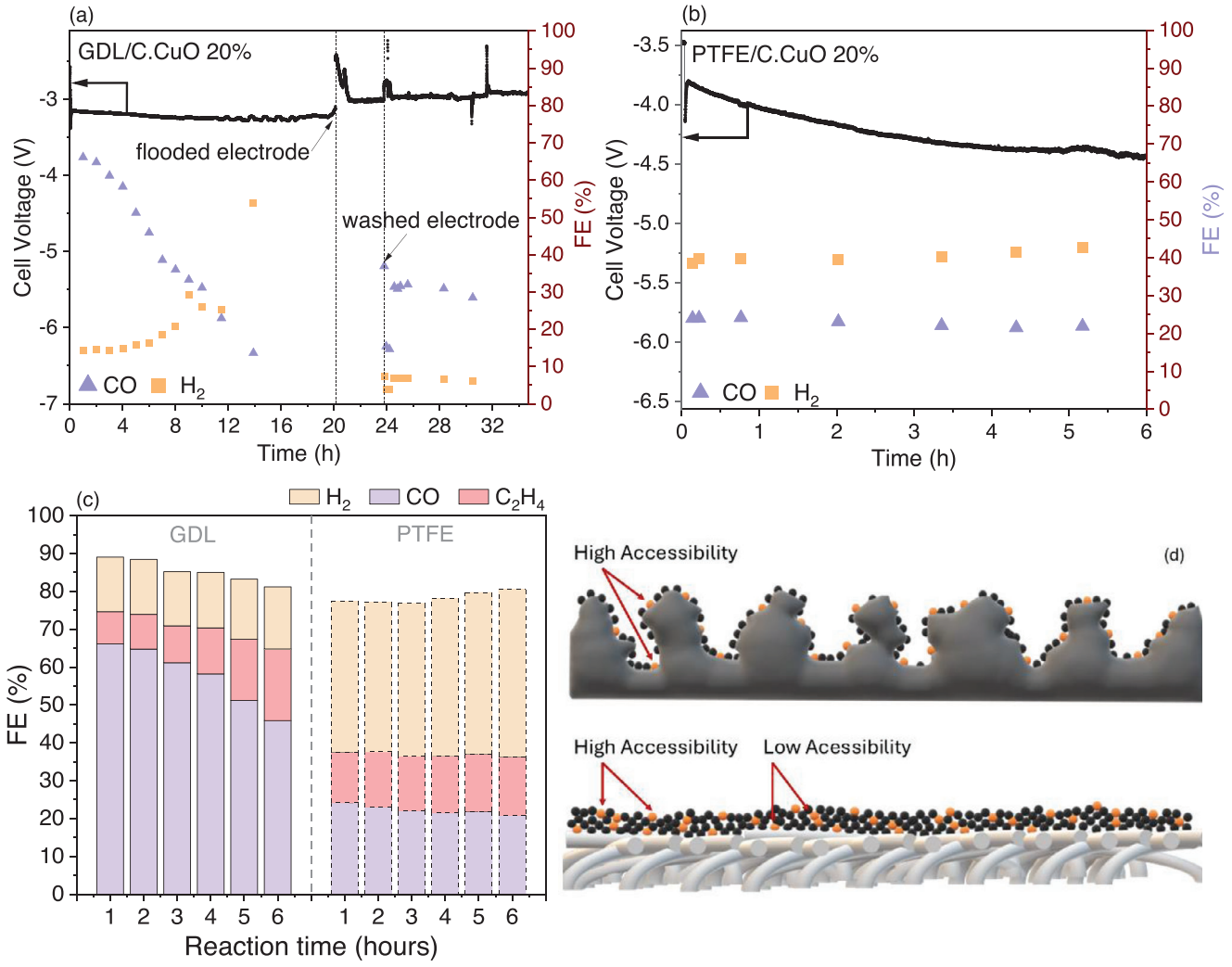

Figure 5. Stability tests for C.CuO 20% on carbon GDL a,c) and PTFE b,c). Catalyst loading on Carbon GDL and PTFE were 1 and 6 mg/cm^2, respectively. Representative scheme of particle dispersion over carbon GDL and PTFE d).

of catalyst is required. The quantity of catalyst was increased (from 1 mg/cm^2 to 6 mg/cm^2) until achieving a better conductivity for the system and obtaining a cell potential similar to those previously obtained, since PTFE is not a conductive material. Despite the catalyst proving to be stable, the results for the first hours were not better than when using carbon GDL, Figure 5c. The FE_{H2} was close to 45%, and in 6 hours, FE for products derived from CO_2 reduction changed from FE_{CO} = 24% to 21% and FE_{C2H4} = 12% to 16%. At the same current range shown in Figure 4, the FE was the same for all of them: FE_{H2} = 45% and FE_{CO} = 34%. The lower catalyst performance could be due to the low roughness found in the PTFE surface, Figure 5d. When the catalyst is sprayed onto a smoother surface, the particles have less surface area for deposition and tend to cover each other. This results in the covered particles becoming less active, as CO_2 has difficulty accessing them, thereby favoring H_2 production. Comparing carbon GDL and PTFE systems, their results suggested that an optimized substrate for this type of low-loading and well-dispersed catalyst is essential, and the optimum option can be a GDL with stable hydrophobicity, high roughness, and good conductivity. These characteristics can guarantee high CO_2 availability and avoid electrode flooding.

Based on the data obtained in this work, we conducted a comprehensive review of the literature concerning the use of copper nanoparticles as catalysts in MEA systems for the electroreduction of CO_2 to CO, as detailed in Table S3. Out of 35 listed articles, only 7 presented results for the desired system, and most did not show significant outcomes for CO formation. Notably, only two of these studies reported Faradaic efficiencies for CO of 65% and 60%, utilizing commercial Cu nanoparticles and CuO nanosheets, respectively. Our system, despite employing a minimal amount of catalyst, achieved results comparable to or even surpassing those reported in the literature, highlighting its efficiency and potential.

3. Conclusion

In conclusion, the exploration of ECR using low-Cu-nanoparticle content has provided valuable insights for enhancing catalytic

performance. A comparative analysis with established literature results, confirms that our approach yields highly competitive performance with other catalysts, demonstrating that copper is a viable option for replacing silver in CO production. The study underscores that the catalyst's efficiency is intricately linked to the substrate, emphasizing that the way CO_2 accesses the catalyst sites plays a crucial role; the quantity of the catalyst does not solely determine it. The study highlights that the loss of hydrophobicity and low roughness in a substrate can significantly impact the catalyst's performance, emphasizing the need to develop an improved substrate for this MEA-cell configuration. Such an optimized substrate is vital to ensuring stability and conductivity, enhancing the overall effectiveness of the CO_2 reduction process.

4. Experimental Section

Catalyst synthesis: The materials were prepared following a technique previously reported.[39] In brief, appropriate amounts of CB (Vulcan XC-72, Cabot) were dispersed in a solution of Cu acetate (Sigma-Aldrich, 99.0%) in ethanol (99.5%) within the PTFE liner of an autoclave vessel and stirred for 10 minutes. The autoclave vessel was then sealed and heated at 110 °C for 12 hours. Afterward, the resulting solids were washed and centrifuged three times in ethanol until a transparent solution was achieved. Subsequently, the CB/CuO powders were dried overnight at 60 °C. CB/CuO samples were then prepared with varying weighted ratios of CuO on CB (ranging from 0 to 60 wt %). The samples with weight ratios of CB to CuO at 0 (representing bare CB), 10, 15, 20, 40, and 60 wt% are designated as C, C.CuO 10%, C.CuO 15%, C.CuO 20%, C.CuO 40%, and C.CuO 60%, respectively.

Physical Characterization: The synthesized catalysts (Cu over carbon black) were characterized by XRD using a Shimadzu XRD-600 equipped with Cu-Kα radiation (λ = 1,5406 Å) and a scan rate of 2°/min from 10 to 80° (2θ). The morphology characterization was made using transmission electron microscopy (JEM-2100-JEOL LaB6) and SEM (FEI Magellan 400 L-FEG). TGA and DSC measurements were done in a TGA–Q500 (Instruments, New Castle, DE) with a heating ramp of 10° C/minutes from 25 to 800 °C.

Electrochemical CO_2 reduction: Electrochemical experiments were conducted on membrane electrode assemblies (MEA) cells, as shown in Figure S9. The electrodes were prepared by spraying an ink (5 mL of methanol P.A., 10 mg of catalyst, and 80 mL of Nafion resin solution – 5% Sigma Aldrich) onto a 2 cm x 1 cm carbon GDL or polytetrafluoroethylene membrane (PTFE – with a pore size of 0.45 microns), keeping 1 mg/cm^2 of catalyst on carbon GDL and 6 mg/cm^2 on PTFE. The anode used was prepared with 1 mg/cm^2 of IrO2 by drop-casting onto titanium felt (2 cm^2). The anode used for the stability test was a sputtered IrO2 on titanium felt. The cathode and anode in the MEA cell were separated by an AEM, Sustainion-Dioxide Materials, and a PTFE gasket to avoid contact between them. The exposed geometric area for the electrodes was 2 cm^2. Experiments were controlled using a potentiostat (Autolab). A peristaltic pump was used to recirculate the anolyte (0.1 M $KHCO_3$) at a flow rate of 40 mL/min. Humidified CO_2 (Praxair, high purity 5.0) was flown through the cathode at a flow rate of 30 standard cubic centimeters per minute (sccm) controlled by an electronic mass controller. The flow rate was measured in the outlet and used to calculate the FE. The electrochemical cell outlet was connected in line with the gaseous chromatograph (GC, PerkinElmer Clarus 590) for quantification. A molecular sieve (5A–Supelco) was used for CO and H_2 separation, leading the gas flow to a thermal conductivity detector (TCD) running at 250° C. For the hydrocarbon separation, a Carboxen-1000 packed column was used, connected to a Flame Ionization Detector (FID). Both columns were kept at 180° C. Argon was used as a carrier gas (flow rate–20 sccm). Liquid products were analyzed by Nuclear Magnetic Resonance (NMR) using 600 Hz Bruker equipment at 25° C. A presaturated method, water suppression, and a mix of H_2O-D_2O 90:10 and Dimethylsulfoxide (DMSO) as an internal standard were used for quantification.[40]

The FE was calculated using the following equation.

$$FE\ (\%) = \frac{m.n.F}{I.t}$$

where m is the number of mols of obtained products, n is the number of electrons to convert CO_2 to the desired product, F is the Faraday's constant (96485 C/mol), I is the applied current (ampere), and t is the reaction time (s).

Supporting Information

The authors have cited additional references within the Supporting Information.[41–47] The Supporting Information includes additional characterizations, experimental results, and comparative data from the literature to further support the findings presented in the main manuscript.

Acknowledgments

E. H. Dias would first like to be grateful to God. E. H. Dias, G. T. S. T. da Silva, C. R. de Oliveira, and L. H. Mascaro gratefully acknowledge the financial support given by FAPESP (2018/01258–5, 2019/10689–2, 2022/16560–4, 2022/10255–5, and 2023/10268–2, 2013/07296–2, 2017/11986-5), Laboratório de Caracterização Estrutural (LCE) for the SEM analysis, Central de Análises Químicas Instrumentais (CAQI) for the TEM analysis and FINEP iTechAgro (01.24.0554.00) for the infrastructure. The authors also acknowledge the support of the Brazilian S&T&I Ministry through SISH2 (CNPq # 407878/2022–0), BRICS (CNPq # 4440117/2022-4) and INCT Programs (CNPq # 406925/2022–4).

The Article Processing Charge for the publication of this research was funded by the Coordenaçáo de Aperfeiçoamento de Pessoal de Nível Superior - Brasil (CAPES) (ROR identifier: 00x0ma614).

Conflict of Interest

The authors declare no conflict of interests.

Data Availability Statement

The data that support the findings of this study are available from the corresponding author upon reasonable request.

Keywords: AEM-Cell · CO production · CO_2 reduction · copper nanoparticles · electrochemical

[1] Z. Yin, D. Gao, S. Yao, B. Zhao, F. Cai, L. Lin, P. Tang, P. Zhai, G. Wang, D. Ma, X. Bao, *Nano Energy* **2016**, *27*, 35.
[2] F. Nocito, A. Dibenedetto, *Curr. Opin. Green Sustain. Chem.* **2020**, *21*, 34.
[3] R. W. Howarth, M. Z. Jacobson, *Energy Sci. Eng.* **2021**, *9*, 1676.
[4] S. M. Jordaan, C. Wang, *Nat. Catal.* **2021**, *4*, 915.
[5] L. Yuan, S. Zeng, X. Zhang, X. Ji, S. Zhang, *Mater. Rep. Energy* **2023**, *3*, 100177.
[6] Y. Zheng, A. Vasileff, X. Zhou, Y. Jiao, M. Jaroniec, S. Z. Qiao, *J. Am. Chem. Soc.* **2019**, *141*, 7646.
[7] A. Vasileff, C. Xu, Y. Jiao, Y. Zheng, S.-Z. Qiao, *Chem* **2018**, *4*, 1809.
[8] P. Iyengar, J. Huang, G. L. De Gregorio, C. Gadiyar, R. Buonsanti, *Chem. Commun.* **2019**, *55*, 8796.
[9] M. Sassenburg, R. de Rooij, N. T. Nesbitt, R. Kas, S. Chandrashekar, N. J. Firet, K. Yang, K. Liu, M. A. Blommaert, M. Kolen, D. Ripepi, W. A. Smith, T. Burdyny, *ACS Appl. Energy Mater.* **2022**, *5*, 5983.
[10] D. Cheng, Z. J. Zhao, G. Zhang, P. Yang, L. Li, H. Gao, S. Liu, X. Chang, S. Chen, T. Wang, G. A. Ozin, Z. Liu, J. Gong, *Nat. Commun.* **2021**, *12*, 395.
[11] Y. Lum, J. W. Ager, *Nat. Catal.* **2019**, *2*, 86.
[12] T. Cheng, H. Xiao, W. A. Goddard, *J. Am. Chem. Soc.* **2017**, *139*, 11642.
[13] X. Xiao, Y. Xu, X. Lv, J. Xie, J. Liu, C. Yu, *J. Colloid Interface Sci.* **2019**, *545*, 1.
[14] N. M. Latiff, X. Fu, D. K. Mohamed, A. Veksha, M. Handayani, G. Lisak, *C N Y* **2020**, *168*, 245.
[15] O. A. Baturina, Q. Lu, M. A. Padilla, L. Xin, W. Li, A. Serov, K. Artyushkova, P. Atanassov, F. Xu, A. Epshteyn, T. Brintlinger, M. Schuette, G. E. Collins, *ACS Catal.* **2014**, *4*, 3682.
[16] M. Jia, C. Choi, T. S. Wu, C. Ma, P. Kang, H. Tao, Q. Fan, S. Hong, S. Liu, Y. L. Soo, Y. Jung, J. Qiu, Z. Sun, *Chem. Sci.* **2018**, *9*, 8775.
[17] A. K. Buckley, S. Ma, Z. Huo, T. Z. Gao, K. P. Kuhl, *Nat. Nanotechnol.* **2022**, *17*, 811.
[18] A. Del Castillo, M. Alvarez-Guerra, J. Solla-Gullón, A. Sáez, V. Montiel, A. Irabien, *Appl. Energy* **2015**, *157*, 165.
[19] H. R. Q. Jhong, F. R. Brushett, P. J. A. Kenis, *Adv. Energy Mater.* **2013**, *3*, 589.
[20] Y. Jang, C. Seol, S. M. Kim, S. Jang, *Int. J. Hydrogen Energy* **2022**, *47*, 18229.
[21] B. Zhang, J. Zhang, P. An, Z. Su, Q. Wan, X. Tan, L. Zheng, *Nano Energy* **2021**, *88*, 106239.
[22] J. W. Blake, J. W. Haverkort, J. T. Padding, *Electrochim. Acta* **2024**, *507*, 145177.
[23] P. Iyengar, M. J. Kolb, J. Pankhurst, F. Calle-Vallejo, R. Buonsanti, *ACS Catal.* **2021**, *11*, 13330.
[24] R. Reske, H. Mistry, F. Behafarid, B. Roldan Cuenya, P. Strasser, *J. Am. Chem. Soc.* **2014**, *136*, 6978.
[25] K. M. El Khatib, R. M. Abdel Hameed, *Biosens. Bioelectron.* **2011**, *26*, 3542.
[26] Q. Li, L. Wu, G. Wu, D. Su, H. Lv, S. Zhang, W. Zhu, A. Casimir, H. Zhu, A. Mendoza-Garcia, S. Sun, *Nano Lett.* **2015**, *15*, 2468.
[27] S. Ren, D. Joulié, D. Salvatore, K. Torbensen, M. Wang, M. Robert, C. P. Berlinguette, *Science 1979* **2019**, *365*, 367.
[28] S. Verma, Y. Hamasaki, C. Kim, W. Huang, S. Lu, H. R. M. Jhong, A. A. Gewirth, T. Fujigaya, N. Nakashima, P. J. A. Kenis, *ACS Energy Lett.* **2018**, *3*, 193.
[29] D. Gao, I. T. McCrum, S. Deo, Y.-W. Choi, F. Scholten, W. Wan, J. G. Chen, M. J. Janik, B. R. Cuenya, *ACS Catal.* **2018**, *8*, 10012.
[30] J. Lai, W. Niu, R. Luque, G. Xu, *Nano Today* **2015**, *10*, 240.
[31] S.-M. Lee, S.-H. Lee, J.-S. Roh, *Crystals (Basel)* **2021**, *11*, 153.
[32] C. F. Holder, R. E. Schaak, *ACS Nano* **2019**, *13*, 7359.
[33] B. Akbari, M. Pirhadi Tavandashti, M. Zandrahimi, *Iran. J. Mater. Sci. Eng* **2011**, *8*.
[34] A. Aslani, *Phys. B Condens. Matter* **2011**, *406*, 150.
[35] M. Ghosh, C. N. R. Rao, *Chem. Phys. Lett.* **2004**, *393*, 493.
[36] A. Aslani, V. Oroojpour, *Phys. B Condens. Matter* **2011**, *406*, 144.
[37] H. Siddiqui, M. S. Qureshi, F. Z. Haque, *Optik (Stuttg)* **2016**, *127*, 4726.
[38] S. Feng, Z. Zhong, Y. Wang, W. Xing, E. Drioli, *J Memb. Sci.* **2018**, *549*, 332.
[39] E. H. Dias, G. T. S. T. Da Silva, J. C. Da Cruz, C. Ribeiro, *ChemElectroChem* **2022**, *9*, e202200206.
[40] T. Chatterjee, E. Boutin, M. Robert, *Dalton Trans.* **2020**, *49*, 4257.
[41] P. Ding, J. Kühne, S. Santra, R. Zell, P. Zellner, T. Rieth, J. Gao, J. Chen, G. Zhou, J. Dittloff, *Adv. Energy Mater.* **2024**, 14 2303936.
[42] E. Cho, J. Nam, D. H. Won, J.-S. Yu, J. Kim, S.-Y. Jang, Y. J. Hwang, *J. Mater. Chem. A* **2022**, *10*, 10363.
[43] T. Ito, J. Raj, T. Zhang, S. Roy, J. Wu, *EES Catal.* **2024**, *2*, 997.
[44] D. Kim, H. Yun, J. Kim, C. W. Lee, Y. J. Hwang, *J. Mater. Chem. A* **2024**, *12*, 23780.
[45] P. Wei, D. Gao, T. Liu, H. Li, D. Li, H. Liu, R. Sun, X. Li, Y. Li, M. Lin, X. Zang, Q. Wang, H. Hu, B. Xi, J. Zhang, H. Wu, J. Wu, Y. Li, C. M. Li, J. Lu, X. Sun, *Nat. Nanotechnol.* **2023**, *18*, 291.
[46] Y.-H. Huang, X.-X. Li, W.-H. Li, L.-Y. Hao, J.-Q. Yu, J.-B. Jia, Y.-N. Huang, *Small* **2024**, *20*, e2400441.
[47] N.-H. Tran, H. P. Duong, G. Rousse, S. Zanna, M. W. Schreiber, M. Fontecave, *ACS Appl. Mater. Interfaces* **2022**, *14*, 31933.

Manuscript received: June 4, 2025
Revised manuscript received: June 19, 2025
Version of record online: ■■, ■■

RESEARCH ARTICLE

A few copper nanoparticles (less than 1 mg/cm^2) supported on CB and deposited on a carbon-based GDL can achieve Faradaic efficiencies exceeding 60% for CO formation at 100 mA/cm^2 due to their homogeneous dispersion and separated catalytic sites.

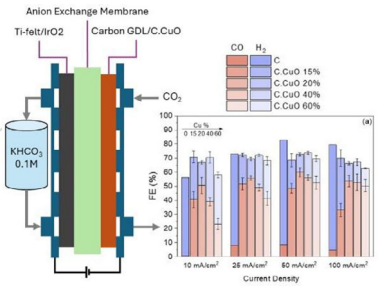

E. H. Dias, G. T. dos S. T. da Silva, C.-T. Dinh, K. H. Dinh, L. H. Mascaro, C. Ribeiro

1 – 8

High Dispersion of Copper Nanoparticles on Carbon Black in Minimal Loadings Enhances the Electroreduction of CO_2 to CO